Hematite microdisks as an alternative anode material for lithium-ion batteries

Suresh Kannan Balasingam[a±], Manab Kundu[a±≠*], Balamuralitharan Balakrishnan[b], Hee-Je Kim[b], Ann Mari Svensson[a], Kaushik Jayasayee[c*]

[a]*Department of Materials Science and Engineering, Norwegian University of Science and Technology (NTNU), Trondheim-7491, Norway*
[b]*School of Electrical and Computer Science Engineering, Pusan National University, Busan-46241, Republic of Korea*
[c]*Department of Sustainable Energy Technology, SINTEF Industry, Trondheim-7491, Norway*

Abstract

In this work, hematite microdisks (500 nm to 1μm in diameter, ~200 nm in thickness) have been synthesized by a facile hydrothermal method which exhibited good cycling stability at a current density of 200 mA g^{-1} and 1000 mA g^{-1}, and excellent rate performance at various current densities ranging from 100 mA g^{-1} to 4000 mA g^{-1}.

Keywords: Hematite microdisks; Li-ion battery; high specific capacity; anode

± These authors contributed equally

≠ *Present address: SRM Research Institute, Department of Chemistry, SRM Institute of Science and Technology, Chennai-603203, India*

*Corresponding authors
E-mail address: chemmanab@gmail.com (M. Kundu), kaushik.jayasayee@sintef.no (K. Jayasayee)

1. Introduction

In response to the development of an alternative LIB anode material with high specific capacity and good cycling stability, various transition metal oxides (Fe_2O_3, NiO, CuO, Co_3O_4, MnO_2 etc.) has been explored and extensively studied [1]. Among them, hematite (Fe_2O_3) with very high theoretical capacity (1007 mAh g^{-1}), non-toxic nature and six times higher volumetric capacity than that of graphite (5.24 g cm^{-3} for Fe_2O_3 vs. 2.16 g cm^{-3} for graphite) has been explored extensively [2-8]. However, the large volume changes during the

electrochemical lithiation/delithiation process leads to poor capacity retention, which limits its practical applications.

To resolve these issues, various strategies such as minimization of particle size and amplification of specific surface area, designing highly porous structure, encapsulating Fe_2O_3 in three dimensional conductive carbon network has been attempted [9-11]. Because of the high surface to volume ratio, reduced Li-ion diffusion path and improved electronic conductivity, these nanostructured LIB anodes confirmed their improved lithium storage properties. For example, Wang et al. reported nanostructured α-Fe_2O_3 electrode, which delivers a high reversible capacity of 1239.2 mAh g^{-1} at 1 C even after 500 cycles and a discharge capacity of 513.3 mAh g^{-1} at 10 C [11].

Unfortunately, these nanostructured materials with unique architectural features cannot be commercially used as battery materials because of the difficulties in handling nano-powders and achieving a high tap density [12]. Even though tap density is one of the key aspects for processing of anodes, as well as for achieving high energy density of the final device, so far only limited interest have been paid to develop high tap density LIB anode materials [13].

In this work, to achieve interesting balance between high rate and high tap density, we have synthesized hematite microdisks (500 nm to 1μm in diameter, ~200 nm in thickness) by a facile hydrothermal method. The unique microstructural feature of Fe_2O_3 microdisks demonstrate that they could tolerate the volume change and structural destruction of the electrodes during repeated electrochemical lithiation/delithiation process.

2. Result and Discussion:

The detail experimental procedure for the synthesis of hematite microdisks, physico-chemical and electrochemical characterization methods are provided in the electronic supporting information (ESI). Fig. 1a shows the SEM image of as-synthesized α-Fe_2O_3 microdisks with
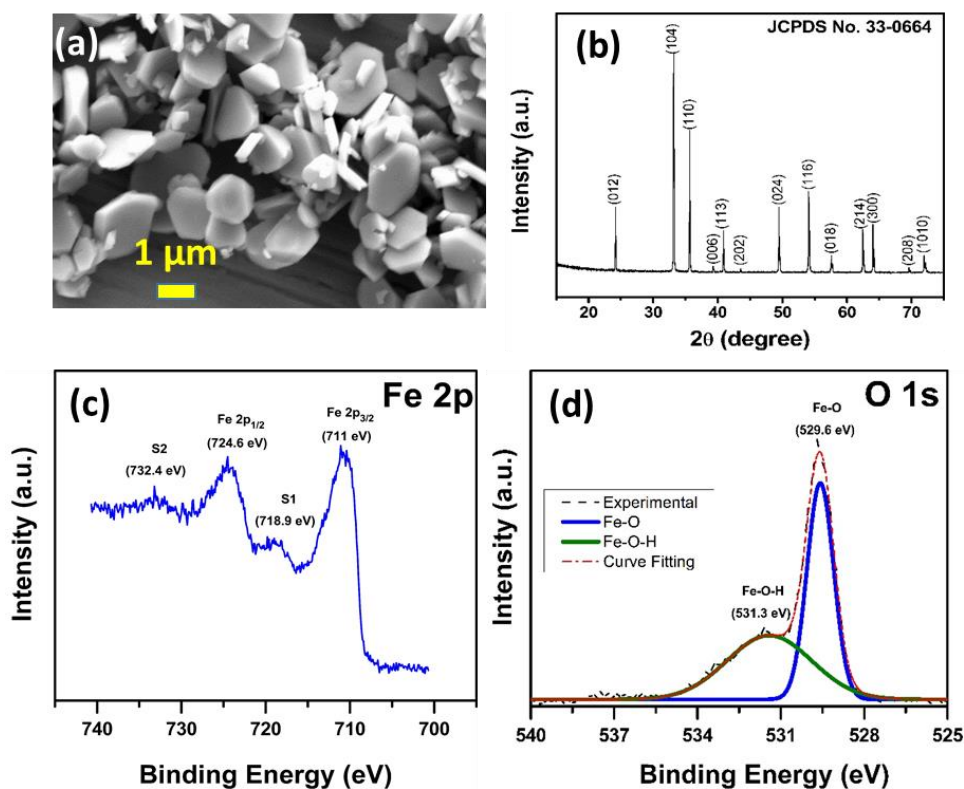
Figure 1. (a) SEM image of α-Fe₂O₃ microdisks; (b) XRD patten of the as-synthesized material; (c) core-level XPS spectrum of Fe 2p; and (d) core-level XPS spectrum of O 1s

various size distribution in the range of 0.5 to 1 μm. The vertically scattered microdisks show the average thickness of around 200 nm, which is confirmed by the high magnification FE-SEM image (see Fig. S1, ESI). Fig. 1b shows the diffraction pattern of hematite structure which is well matched with the standard pattern (JCPDS No. 33-0664). All the main diffraction peaks of α-Fe₂O₃ can be indexed as rhombohedral crystal structure with R$\overline{3}$C space group, the sharp diffraction peaks confirm the formation of highly crystalline hematite phase and the absence of additional peaks further confirms the formation of phase pure material [14]. Fig. 1c shows the core-level XPS spectra of Fe 2p. The two major peaks appear at 711 and 724.6 eV corresponds to the $2p_{3/2}$ and $2p_{1/2}$ orbitals, respectively. Also, two satellite peaks S1 and S2 appear at binding energies of 718.9 and 732.4 eV, respectively [15]. The O 1s core-level spectrum is shown in Fig. 1d in which the main Fe-O peak appears at a

binding energy of 529.6 eV and the auxiliary peak appear at a binding energy of 531.3 eV corresponds to the Fe-O-H bonding due to the surface adsorbed water molecules [15]

Figure 2a. represents the first four CV curves at a scan rate of 0.2 mV s^{-1}. The strong lithiation peak appears in the 1st cycle at ~0.57 V is due to the reduction of Fe^{3+} to Fe^0, the reaction of Li with Fe to form Li_xFe_y alloys, and the formation of solid electrolyte interface (SEI) layer [16]. In this step, generation of amorphous Li_2O and SEI formation are the foremost reason of the irreversible capacity loss [17]. Contrary, during the delithiation, process the main peak at ~1.67 V corresponds to the reversible oxidation of Fe^0 to Fe^{3+} [18]. After the second cycles onwards, the shifting of lithiation peak at 0.57 V to higher potential at 0.92 V is associated with the kinetics of the electrode reactions, possibly due to the activation of electroactive material during the first cycle [19, 20]. The lithiation/delithiation of mechanism of various transition metal oxides including Fe_2O_3 follow conversion mechanism, which is briefly explained in previous reports [1, 21, 22].

Figure 2b represents the potential profiles of the α-Fe_2O_3 electrode at a rate of 200 mA g^{-1} for various cycle number. For the 1st cycle lithiation process, a flat potential plateau at ~ 0.8 V is observed followed by a long slope. This flat plateau is related to the conversion of Fe^{3+} to Fe^0 and the formation of SEI layer on the surface of electrode. The observed delithiation capacities of Fe_2O_3 electrode in the 1st, 2nd, 3rd, 10th, 50th and 100th cycles are 705.55, 639.66, 621.3, 570.83 and 483.168 and 476.14 mAhg^{-1}, respectively. After the 1st cycle, the efficiency increases with the cycle number and reaches to ~99%. The low initial coulombic efficiency (55.27 %) is due to the irreversible reaction of electrode material with the electrolyte and formation of SEI layer on the surface of electrode materials, this phenomenon is common for other transition metal oxides too [23]. Moreover, very similar potential hysteresis after first cycle onwards can be attributed to the good reversibility of the conversion reaction of Fe_2O_3 with Li and smooth kinetics of solid state Li-ion diffusion

through the electrode materials during the electrochemical lithiation/delithiation process. The cycling performances of the Fe_2O_3 electrode is measured at a current density of 200 mAhg^{-1} and shown in Figure 2c. The fading in specific capacity value with the cycle number is well agreed with the reduction in peak intensity with the cycle number in CV. Moreover, the Fe_2O_3 electrode delivers an excellent reversible capacity of 476 mAhg^{-1} even after 100 cycles.
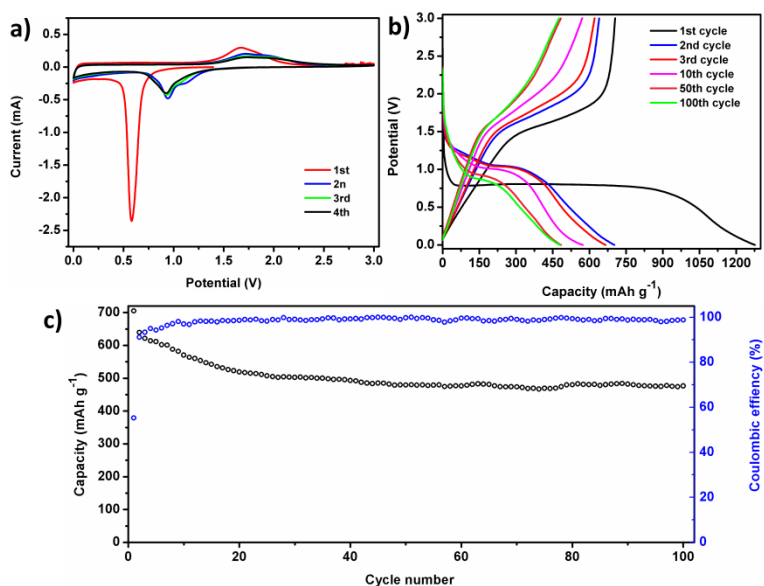
Figure 2. Cyclic voltammograms at a scan rate of 0.2 mVs^{-1} (a), Charge-discharge at 200 mA g^{-1} within a voltage range of 0.0–3.0 V (b), evaluation of discharge capacity vs. cycle number at the current density of 200 mA g^{-1} (c).

Figure 3a represents the rate performance of Fe_2O_3 electrode at different applied current densities (ranging from 100 mA g^{-1} to 4000 mA g^{-1}). The Fe_2O_3 electrode delivers the delithiation capacities of 722.7-576.47, 513.2-469.748, 406.55-369.34 and 347.5-329.3 mAh g^{-1} at the current densities of 100, 200, 500 and 1000 mAg^{-1}, respectively. Also, a good reversible capacity of 254 mAhg^{-1} and 210 mAhg^{-1} could be maintained when the current density increased to 2000 and 4000 mAh g^{-1}. When the current density was reduced back to 200 mAhg^{-1}, the sample could still keep a high and stable reversible capacity of 424 mAh g^{-1},

indicates good rate performance and reversibility. The potential profiles at the various current densities are shown in Fig. 3b. Irrespective of current densities, the plateaus corresponding to lithiation and delithiation could be seen evidently. Such impressive lithium storage behavior of Fe_2O_3 electrode even at a very high current density (2000 mA g^{-1} and 4000 mA g^{-1}) implies that this type of electrode could serve as a promising candidate for high power applications.
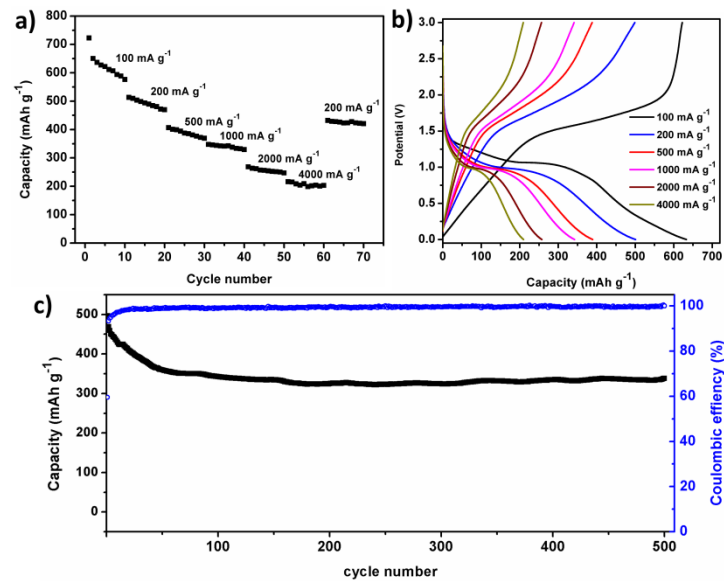

Figure 3. Variation in discharge capacity with the cycle number at different current densities (ranging from 100 to 4000 mA g^{-1}) (a), Charge-discharge curves at the corresponding current density (b), long term cycling test at the current density of 1000 mA g^{-1}.

4. Conclusions

In summary, Fe_2O_3 microdisks with the size distribution in the range of 0.5 to 1 μm and the average thickness of around 200 nm were synthesized via hydrothermal method. While evaluating lithium storage performance, Fe_2O_3 electrode shows excellent electrochemical performance in terms of specific capacity, rate capability at various applied current densities (ranging from 100 to 4000 mA g^{-1}) and cycle stability at 200 mA g^{-1} and 1000 mA g^{-1}.

References

[1] K. Cao, T. Jin, L. Yang, L. Jiao, Mater. Chem. Front. 1 (2017) 2213-2242.

[2] T.-Y. Kim, S. Park, Y. Yoon, J.-H. Lee, J. Jeon, M.S. Kim, Y. Kim, M.G. Kim, H.-G. Hur, ACS Applied Materials & Interfaces (2019).

[3] J. Sun, C. Lv, F. Lv, S. Chen, D. Li, Z. Guo, W. Han, D. Yang, S. Guo, ACS Nano 11 (2017) 6186-6193.

[4] F. Han, D. Li, W.-C. Li, C. Lei, Q. Sun, A.-H. Lu, Adv. Funct. Mater. 23 (2013) 1692-1700.

[5] Y. Chen, X. Zhao, Y. Liu, A.A. Razzaq, A.K. Haridas, K.-K. Cho, Y. Peng, Z. Deng, J.-H. Ahn, Electrochim. Acta 289 (2018) 264-271.

[6] N. Wu, X. Zhang, C. Ma, Y.-R. Shi, J.-M. Zhou, Z. Wang, H. Liu, X.-X. Zeng, Y. Wei, Electrochimica Acta 297 (2019) 1028-1034.

[7] M. Kundu, G. Karunakaran, N. Van Minh, D. Kuznetsov, J. Clust. Sci. 28 (2017) 1285-1293.

[8] Y. Li, Y. Huang, Y. Zheng, R. Huang, J. Yao, Journal of Power Sources 416 (2019) 62-71.

[9] J. Li, K. Sun, C. Leng, J. Jiang, RSC Adv. 8 (2018) 37417-37423.

[10] H. Wang, Y. Song, Y. Li, M. Wang, Q. Ma, W. Yu, D. Li, X. Dong, J. Wang, G. Liu, RSC Adv. 8 (2018) 30794-30801.

[11] Y. Wang, J. Roller, R. Maric, J. Power Sources 378 (2018) 511-515.

[12] J.S. Cho, Y.J. Hong, J.-H. Lee, Y.C. Kang, Nanoscale 7 (2015) 8361-8367.

[13] Z.-D. Huang, T.-T. Zhang, H. Lu, T. Masese, K. Yamamoto, R.-Q. Liu, X.-J. Lin, X.-M. Feng, X.-M. Liu, D. Wang, Y. Uchimoto, Y.-W. Ma, Energy Storage Mater. 13 (2018) 329-339.

[14] D. Peng, S. Beysen, Q. Li, Y. Sun, L. Yang, Particuology 8 (2010) 386-389.

[15] X.-F. Lu, X.-Y. Chen, W. Zhou, Y.-X. Tong, G.-R. Li, ACS Applied Materials & Interfaces 7 (2015) 14843-14850.

[16] Z. Na, G. Huang, F. Liang, D. Yin, L. Wang, Chem. Eur. J. 22 (2016) 12081-12087.

[17] H. Liu, G. Wang, J. Wang, D. Wexler, Electrochem. Commun. 10 (2008) 1879-1882.

[18] H. Liang, W. Chen, Y. Yao, Z. Wang, Y. Yang, Ceram. Int. 40 (2014) 10283-10290.

[19] L. Jin, X. Chunhui, C. Xu, G. Ruixia, D. Shujiang, Nanotechnology 27 (2016) 215403.

[20] C. Wu, H. Zhang, Y.-X. Wu, Q.-C. Zhuang, L.-L. Tian, X.-X. Zhang, Electrochimica Acta 134 (2014) 18-27.

[21] K. Cao, L. Jiao, H. Xu, H. Liu, H. Kang, Y. Zhao, Y. Liu, Y. Wang, H. Yuan, Advanced Science 3 (2016) 1500185.

[22] Q. Sun, Z. Wang, Z. Zhang, Q. Yu, Y. Qu, J. Zhang, Y. Yu, B. Xiang, ACS Applied Materials & Interfaces 8 (2016) 6303-6308.

[23] S. Chen, Y. Xin, Y. Zhou, F. Zhang, Y. Ma, H. Zhou, L. Qi, J. Mater. Chem. A 3 (2015) 13377-13383.